Low Energy Uniformity of the HRC-I Quantum Efficiency

R. H. Donnelly, J. P. Brown, and K. T. Hole

23rd May 2003

1 Introduction

The nominal flat field map of the HRC-I, constructed from subassembly calibration (SAC) data taken at six energies,[1] suggests that at energies above ~183 eV the quantum efficiency (QE) of the HRC-I is uniform across the detector to within ±10% peak to peak, independent of energy.[2] However, observations of the white dwarf HZ 43 show that at $+10'$ off-axis there is a significant deviation from the nominal QE uniformity (QEU) at energies below 200 eV. This memo describes our attempt to use observations of the Vela supernova remnant (SNR) taken with the HRC-I and with ROSAT's Position Sensitive Proportional Counter (PSPC) to construct a new QEU map for the HRC-I.

2 Analysis of HZ 43 Observations

Since February 2000, observations of HZ 43 have been taken regularly with the HRC-I/LETG on-axis and at various offsets (see Figure 1) to monitor the low-energy response of the detector. Currently, we have five on-axis observations, four observations at $+10'$ off-axis, and one observation each at $-10'$ and $+5'$ off-axis.

To analyze the detector's response at the four locations, we first need to obtain the background-subtracted, zeroth order count rate for each observation. For this analysis, we used the level 1 event lists filtered on the good time intervals (GTIs) given in the level 2 event list headers. We used the level 1 event lists because the event quality filtering done as part of the standard processing to make the level 2 event lists removes up to 5% of source events that are, for reasons not entirely understood, misplaced.[3] This filtering is desirable if one is doing high resolution imaging, but can introduce larger uncertainties in photometric work since the exact amount and positions of rejected events are not known.

[1] B (0.183 keV), C (0.277 keV), O (.525 keV), Al (1.487 keV), Ti (4.511 keV), and Fe (6.404 keV)

[2] *http://cxc.harvard.edu/cal/Hrc/flatfield.html*

[3] See *http://cxc.harvard.edu/cal/Hrc/filter.html* for a discussion of HRC-I filtering issues.

Figure 1: Locations of HZ 43 observations on the HRC-I (shown at roll angle of Vela observation for comparison with future images)

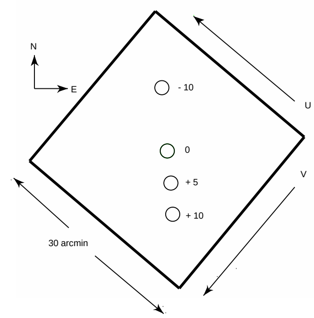

To determine the background-subtracted, zeroth order count rate for each source, we extracted counts in a series of increasingly larger regions surrounding the source. We then examined the total counts as a function of area. The slope of this growth curve represents surface brightness. If the background is approximately uniform, the growth curve should become linear outside of the source. For each observation, we estimated where the growth curve became linear, and then fit a linear least-squares to the data beyond the transition point. The slope of this fit is a direct measurement of the background surface brightness. We then calculated background-corrected counts C_{corr} as a function of area A by the formula

$$C_{corr} = C - b \cdot A$$

where C is the initial total counts within area A and b is the background surface brightness. Next, we did a linear least-squares fit on $C_{corr}(A)$ above the transition point, using the slope of this fit (i.e. corrected background surface brightness) to confirm successful background subtraction, and took the y-intercept as the total source counts. (For an example with ObsID 1000, see Figure 2.) Finally, we divided the total source counts by the exposure time read from the level 2 event list header to get the observed source count rate.

To determine the statistical uncertainty E in the observed count rate, we used the formula

$$E = \frac{\sqrt{C_{tot} + (A_{tot} \cdot E_{bsb})^2}}{t}$$

where C_{tot} is the total number of counts (i.e. the uncorrected counts in the largest circle), t is the exposure time, A_{tot} is the area of the largest circle, and E_{bsb} is the error in the background surface brightness (i.e. the uncertainty in

Figure 2: Finding total observed source counts for ObsID 1000

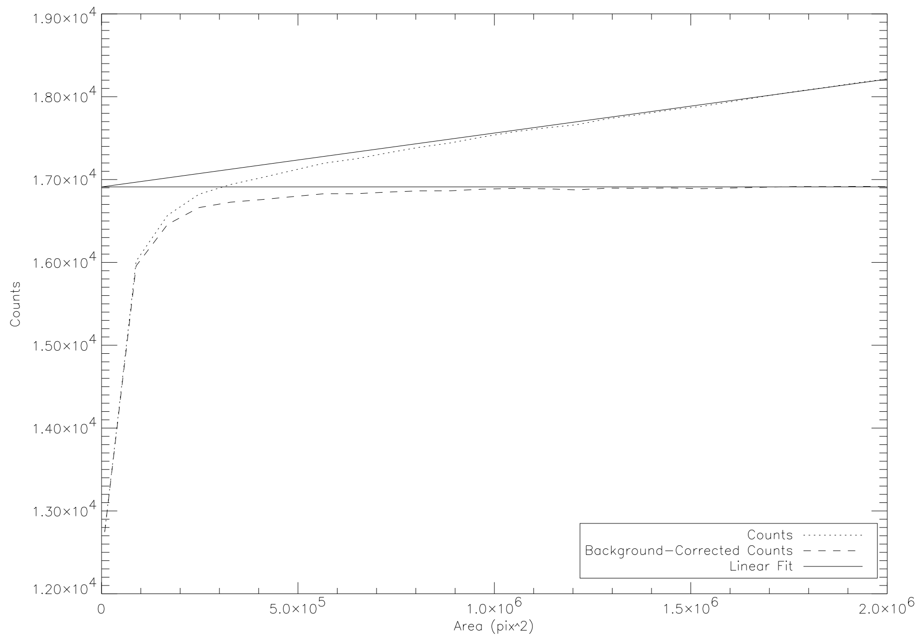

the slope of the original linear least-squares fit). The observed count rates, with statistical uncertainties, are shown in Table 1.

Figure 3 shows an image of the on-axis observation ObsID 1000. The vertical streaks near the top and bottom of the image are the normal first order diffraction and do not concern us in this analysis. However, the centrally located horizontal streaks are zeroth order events that have been dispersed by the fine support structure of the LETG. This diffraction of photons by the fine support structure of the grating complicates the process we have adopted to measure zeroth order count rates: if we include the dispersion streaks in our series of increasingly larger regions, they will make the growth curve non-linear, inflating our estimate of the background surface brightness.[4] To avoid this problem, we used for our extraction rectangular regions centered on the source and perpendicular to the zeroth order streaks. The width of the rectangles was held constant at $\sim 1.75'$, covering the source but excluding the zeroth order streaks. The length of the rectangles was varied from $\sim 0.02' - 17.4'$, stopping a safe distance away from the first order streaks.

The fact that we have excluded the dispersed zeroth order events means that the observed count rates reported here are systematically lower than the true rates by 1-2%. However, since we are studying the detector's uniformity,

[4]If we had enough room to extend the regions far beyond the zeroth-order dispersion streaks, we could treat them as part of the source. However, the presence of first-order streaks puts an upper limit on the region sizes we can use.

Table 1: Observed Count Rates (cts/sec) for HZ 43

Obs ID	Offset (arcmin)	Observed Count Rate (cts/s)
1000	0	4.34±0.04
1001	0	4.44±0.04
1514	0	4.49±0.05
2600	0	4.43±0.06
2602	0	4.33±0.06
1515	+ 5	4.14±0.03
1004	+ 10	3.08±0.02
1516	+ 10	3.04±0.02
2601	+ 10	3.00±0.02
2603	+ 10	2.96±0.02
1005	- 10	3.42±0.02

we are concerned with comparing the relative response of the detector at the four positions with the relative predicted count rates. Thus, the systematic discrepancy between observed and true source count rates will not affect our analysis.

To predict count rates for HZ 43 at the various locations on the detector, we calculated the flux as a function of wavelength, $F(\lambda)$, by the convolution

$$F(\lambda) = S \cdot ISM \cdot A_{eff} \cdot L_0 \cdot QE_0$$

where S is the predicted flux (described in following paragraph); ISM is a photo-electric absorption model using Wisconsin cross-sections; A_{eff} is the on-axis effective area of the HRMA,[5] convolved with a vignetting factor for each off-axis location; L_0 is the LETG zeroth order transmission efficiency;[6] and QE_0 is the on-axis quantum efficiency of the HRC-I (MCP QE[7] times UVIS transmission efficiency[8]), extended down to ~60 eV using an "out of band" response we adapted from data generated by the HRC-I IPI team.

Predicted fluxes were calculated for each observation using two generally accepted HZ 43 models, S_F (Finley) and S_B (Barstow). The total flux was then calculated according to the formula

$$F_{pred} = \frac{\int_{62}^{200} F_F(\lambda) \cdot d\lambda + \int_{62}^{200} F_B(\lambda) \cdot d\lambda}{2}$$

to give the final predicted count rate for each observation, assuming an ideal (i.e. flat) uniformity for the HRC-I. These results are shown in the first column of Table 3.

[5] Latest model in CALDB
[6] Latest model in CALDB
[7] Model v. 2.1
[8] Model v. 4.0

Figure 3: ObsID 1000

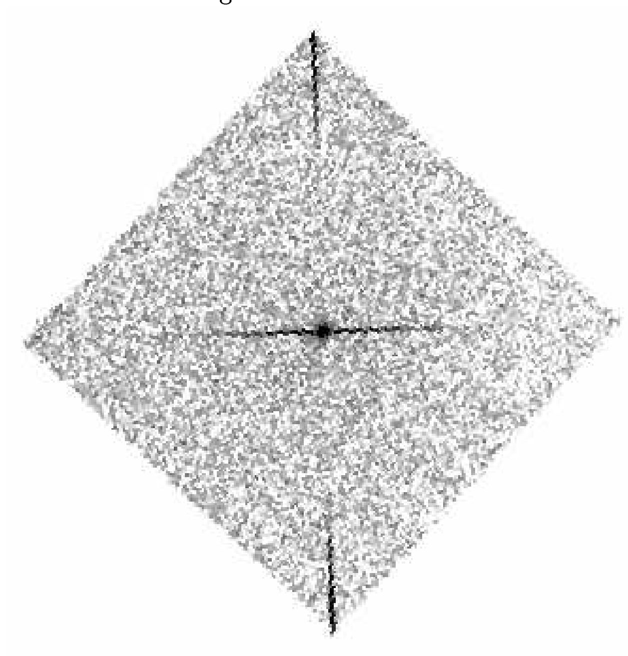

To predict count rates with the current QEU model (version 1.1), we first determined the relative QE at each location by finding the mean value of the v. 1.1 QEU map within a circular region of radius $\sim 1.1'$ centered at that location (i.e. on-axis or offset by $+5'$, $+10'$, or $-10'$). We then multiplied the total predicted flux as determined above by the appropriate QE factor for the location of the observation on the detector. The resulting predictions are shown in the second column of Table 3.

Since HZ 43 radiates primarily below 200 eV, we made a low-energy QEU map by smoothing and normalizing the sum of the B Kα (183 eV) and the C Kα (277 eV) flat field maps taken during SAC. We repeated the steps described in the preceding paragraph to determine the relative QE at each location from this low-energy QEU map and compute predicted count rates. These results are shown in the third column of Table 3.

Many factors contribute to the uncertainty in the predicted count rates - uncertainties in the HRMA effective area and vignetting models, LETG transmission efficiency model, HRC-I QE and QEU models, and uncertainties in the source models for HZ 43. Of these factors, the last dominates: while no error estimate is given for either source model, the two (Barstow and Finley) differ by roughly 20%. Not knowing which source model is more correct, we have averaged the two. Thus, we do not attempt to report accurate uncertainties for our predicted count rates, but note that they must be at least 20%.

A comparison of the normalized predicted count rate (with QEU v. 1.1 and

Table 3: Predicted count rates for HZ 43

Offset	Pred. w/ Ideal QEU	Pred. w/ QEU v. 1.1	Pred. w/ Low-Energy QEU
(arcmin)	($\frac{cts}{s}$)	($\frac{cts}{s}$)	($\frac{cts}{s}$)
0	4.29	4.29	4.29
+ 5	4.02	3.98	4.05
+ 10	3.63	3.51	3.61
- 10	3.73	3.53	3.42

Table 4: Results of HZ 43 analysis, normalized to on-axis values

Offset	Pred. w/ QEU v. 1.1	Pred. w/ Low Energy QEU	Avg. Observed
(arcmin)	($\frac{cts}{s}$)	($\frac{cts}{s}$)	($\frac{cts}{s}$)
0	1	1	1
+ 5	0.93	0.94	0.94
+ 10	0.82	0.84	0.68
- 10	0.82	0.80	0.78

the low-energy QEU) at each offset with the normalized average observed count rate at that offset is shown in Table 4. From this comparison, it is clear that the detector response at $+10'$ off-axis is not correctly modeled by either the current QEU map or the low-energy QEU map. However, note that the maps are adequate for the other positions examined on the detector.

3 Attempting to construct a new QEU map

A raw image obtained with the HRC-I is the convolution of source and sky flux with the telescope response, including mirror effective area and vignetting, and detector quantum efficiency and uniformity. Thus, if we want to construct a map of the detector uniformity, knowing the other elements of the telescope and detector response, in theory all we need to do is divide out the sky and source flux. For this purpose, we attempted to use two observations of the Vela supernova remnant (SNR) taken with ROSAT's PSPC. We hoped to construct the new QEU map based on observations of the Vela SNR because it is very bright below 200 eV, where, as shown by the HZ 43 analysis, the nominal HRC-I QEU map is inadequate. (At higher energies, the nominal QEU model suggests that the detector is uniform to within $\pm 10\%$, and we have not found evidence to the contrary.)

The PSPC field of view is circular, with a radius of about $60'$. The HRC-I field of view is much smaller - approximately $30'$ x $30'$. The PSPC and HRC-I Vela observations are centered on the same celestial coordinates, and the HRC-I field of view is almost entirely inside the central support ring of the PSPC (see Figure 4). This means that the section of the PSPC observation that we are using is located on the most responsive part of the detector and suffers from the

Figure 4: HRC-I FOV inside PSPC central support ring (inverted greyscale)

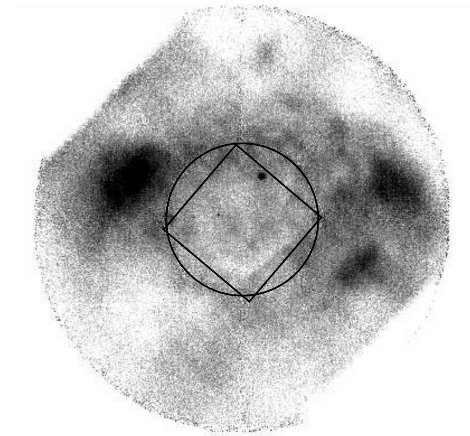

smallest vignetting effects.

Snowden processing on PSPC data removes all telescope and detector effects, as well as non-cosmic background (i.e. particle-induced background, after-pulse events, scattered solar x-ray background, etc.), giving an output image of the source and cosmic background flux.[9] To remove the cosmic background, we used Snowden-processed PSPC observations of AR Lac to construct a background map, which we subtracted from the Snowden-processed Vela images. We added bands 2 through 7 from both PSPC observations, nominally covering an energy range of 0.14 - 2.04 keV. We removed point sources from the image, smoothed it, registered it to the HRC-I image by world coordinates with the IRAF tool *sregister*, and finally normalized it to the central pixel value.

To prepare the HRC-I data, we first used a background map made from HRC-I observations of AR Lac to subtract cosmic and particle background from the Vela image. We then created an exposure map with ideal detector quantum efficiency and spectral weights derived from a source model for Vela.[10] Next, we divided the background-subtracted HRC-I image by this exposure map, removed point sources, and normalized the image to its central value. Finally, we divided this image by the ROSAT image, prepared as described above, to obtain what we hoped would be a map of the HRC-I QEU. The map is shown in Figure 5.

Based on the HZ 43 analysis, we derived expected QEU values at the four locations by dividing the normalized observed count rate at a given location

[9] See the "PSPC Extended Source Cookbook" online at *http://rosat.gsfc.nasa.gov/docs/rosat/cookbook/* and "Analysis Procedures for ROSAT XRT/PSPC Observations of Extended Objects and the Diffuse Background" by Snowden, et al, 1994.

[10] To make the source model, we created a spectrum of the Vela SNR using the pulse invariant (PI) information in the PSPC event lists, and used XSPEC to fit the spectrum with a two temperature Raymond-Smith thermal plasma model with a photo-electric absorption component based on Wisconsin cross-sections.

Figure 5: Attempted QEU map (inverted greyscale)

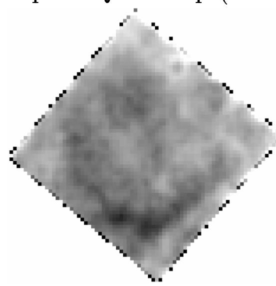

Table 5: Current, Expected, and Derived QEU values

Offset (arcmin)	Current Map	Low Energy Map	Expected QEU value from HZ 43 analysis	QEU value derived from Vela analysis
0	1	1	1	1
+ 5	0.99	1.00	1.00	1.04
+ 10	0.97	0.99	0.81	1.32
- 10	0.95	0.91	0.89	1.09

by the normalized count rate predicted for that location with the most recent on-axis QE model and an ideal QEU. Table 5 shows these expected QEU values, along with the values of the current QEU map, the values of the low-energy QEU map, and the values of our attempted QEU map based on Vela observations. All of the values shown are the mean within a circle of radius $\sim 1.1'$ centered at each location, normalized to the aimpoint, expect for the expected QEU values from the HZ 43 analysis, which are derived as described above. No errors are given because at all locations the statistical uncertainties for the given values are very small: less than 0.1% for the current QEU map, less than 0.2% for the low-energy QEU map, and less than 0.3% for the attempted QEU map derived from the Vela analysis. It is clear from Table 5 that QEU map constructed from Vela observations is very different from what we expect, particularly at $+10'$.

To determine if the features of the attempted QEU map are detector artifacts (from either the HRC-I and/or the PSPC), we performed several tests. First, we looked at a PSPC observation of Vela which has our region of interest in the sky offset from the center of the detector. This image is shown in Figure 7 and the on-aimpoint image is shown in Figure 6. Since the images have the same overall shapes and relative count rates, we conclude that the features of our attempted QEU map are not due to artifacts of the PSPC detector.

As a second test of whether the features in our attempted QEU map are artifacts of the PSPC, we compared PSPC Vela observations in different energy bands. Specifically, we made ratio images of bands 1L (0.11 - 0.284 keV), 3 (0.20 - 0.83 keV), and 4 (0.44 - 1.01 keV) to band 2 (0.14 - 0.284 keV). These ratio images should be free of any detector artifacts the PSPC may have, assuming the artifacts are not strongly energy dependent. However, the anomalies of our

Figure 6: ROSAT image of Vela (inverted greyscale)

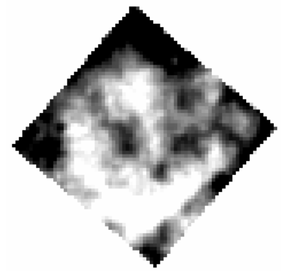

Figure 7: ROSAT image of Vela (same spatial area shown in Figure 6) offset on detector (inverted greyscale)

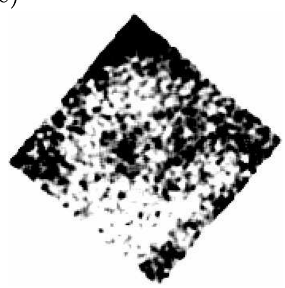

attempted QEU map (Figure 5) are present (though weaker) in each ratio image, reinforcing our conclusion that they are astrophysical features of the SNR, not PSPC artifacts.

As a final test, we compared observations of the Coma Cluster taken with each detector. If the features are due to artifacts of the HRC-I, they should show up when we process and divide the Coma images as we did with the Vela images. However, similar features are not seen (see Figure 8).

In our work to understand the unexpected features of our attempted QEU map, we compared the effective areas of the HRC-I and the PSPC. This com-

Figure 8: Ratio of Coma images (inverted greyscale)

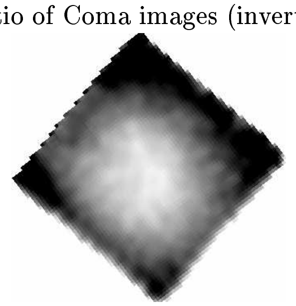

Figure 9: Comparison of Effective Areas

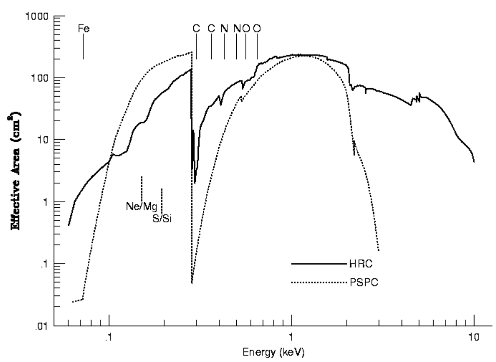

parison is shown in Figure 9. Note that the HRC-I has a greater effective area above the carbon edge and below 100 eV, while the PSPC has a greater effective area between 100 eV and the carbon edge. This means that the HRC-I is more sensitive to emission from iron, carbon, nitrogen, and oxygen, while the PSPC is more sensitive to emission from neon, magnesium, sulphur, and silicon. If there is non-homologous filamentary structure for various elements in the Vela SNR, then the difference in the sensitivities of the two detectors could explain the lumpiness of our attempted QEU map. For example, the bright arc at the bottom corner of our attempted QEU map represents a region that is seen more strongly by the HRC-I than by the PSPC. This region could be a filament that is rich in iron, carbon, nitrogen, or oxygen, or depleted in neon, magnesium, sulphur, or silicon. Since this region covers the $+10'$ offset in the HRC-I observation of Vela, this observation alone is not sufficient to constrain our model of the detector's response. We plan to do another observation of the same field in Vela with the HRC-I at a different roll angle to move this feature of the SNR off the $+10'$ offset, allowing us to determine the relative quantum efficiency at this location.

4 Conclusions

Analysis of HZ 43 observations taken with the HRC-I indicate that at low energies the current QEU map is consistent at $+5'$ and $-10'$ off-axis, but is inaccurate at $+10'$ off-axis. (For other locations on the detector, the validity of the current QEU map at low energies is not known.) We attempted to construct a new QEU map based on observations of the Vela SNR taken with the HRC-I and with ROSAT's PSPC. However, due to differences in the energy response of the two detectors, the PSPC Vela image is not a sufficient flat field for the HRC-I. Specifically, the two detectors see emissions from various lines with different strengths, pointing out a non-homologous filamentary structure of the Vela SNR that persists in our attempted QEU map. Thus, this single HRC-I observation of Vela, while revealing some interesting astrophysical properties of the SNR, is not sufficient to constrain our model of the detector's response at $+10'$. As mentioned earlier, we plan to do another observation of Vela with the HRC-I at a different roll angle. Then we should be able to use the method of comparison with PSPC data, as described in this memo, to measure the relative quantum efficiency of the HRC-I at $+10'$.